Photonic Associative Learning Neural Network based on VCSELs and STDP

Suhong Wang, Shuiying Xiang, Genquan Han, Ziwei Song, Zhenxing Ren, Aijun Wen, and Yue Hao

***Abstract*—In this paper, we propose a photonic neural network (PNN) to emulate associative learning and forgetting for the first time. The PNN contains three photonic neurons based on 1550nm long-wavelength vertical-cavity surface-emitting lasers (VCSELs) subject to double polarized optical injection. A computational model of the PNN is derived based on the well-known spin-flip model. According to the learning rule named spike-time-dependent plasticity (STDP), the connection weight between neurons in the PNN is modified by self-learning. The simulation results show that, during the associative learning process, an association of feeding food and bell ringing is established within the Long-term synaptic potentiation window of the STDP; while, the association is forgotten within the Long-term depression window of the STDP in the forgetting process. Moreover, the effects of time interval between two pre-synaptic spikes on the speed of associative learning and forgetting are considered in detail. Finally, we further realize pattern recall based on the photonic associative learning, which shows promises for emerging applications of a large-scale energy-efficient PNN.**

***Index Terms*—Photonic neural network, vertical-cavity surface-emitting lasers, associative learning and forgetting, spike-time-dependent plasticity, pattern recall**

I. Introduction

NEUROMORPHIC computing has been proposed to numerically emulate the characteristics of the brain to develop the massively parallel and efficient information processing system beyond traditional digital models [1]. With the rapid development of the neuromorphic network, it has a wide range of applications in machine learning and adaptive control, and raises the prospect of brain-like artificial intelligence [2]. In recent years, the photonic neural network (PNN) has become the promising candidate for hardware implementation of ultrafast large-scale brain-inspired computing, due to the profound advantages such as high speed, wide bandwidth, low electromagnetic interference and low power consumption [3].

Manuscript received December 7, 2019. This work was supported in part by the National Natural Science Foundation of China (No. 61974177, 61674119).

S. Y. Xiang is with State Key Laboratory of Integrated Service Networks, Xidian University, Xi'an 710071, China; and also with the State Key Discipline Laboratory of Wide Bandgap Semiconductor Technology, School of Microelectronics, Xidian University, Xi'an 710071, China (e-mail: jxxsy@126.com).

S. H. Wang, Z. W. Song, Z. X. Ren and A. J. Wen are with State Key Laboratory of Integrated Service Networks, Xidian University, Xi'an 710071, China.

Y. Hao and G. Q. Han are with the State Key Discipline Laboratory of Wide Bandgap Semiconductor Technology, School of Microelectronics, Xidian University, Xi'an 710071, China.

In a photonic neuromorphic computing system, the photonic spiking neuron and photonic synapse are essential building elements. Due to the profound virtues of being integrated in two-dimension array easily and coupled to optical fiber efficiently, vertical-cavity surface-emitting lasers (VCSELs) have been widely used to emulate the photonic neurons [4]-[20]. Spike-time-dependent plasticity (STDP) is a fundamental synaptic plasticity mechanism and plays an important role in learning and memory in the human brain [21]-[22]. The STDP has been emulated via various photonic techniques, which satisfies the diverse requirements of neuromorphic computing applications [23]-[30]. For example, semiconductor optical amplifier (SOA) has been widely used to implement photonic STDP [23]-[25]. Photonic STDP based on vertical-cavity semiconductor optical amplifier (VCSOA) is demonstrated to be an energy-efficient approach with much lower power consumption than that based on a conventional SOA [26]. Furthermore, the STDP-based unsupervised spiking pattern learning in a photonic spiking neural network with VCSELs and VCSOAs was predicted in our previous work [27].

Note, associative learning and forgetting processes are of vital importance for logical thinking and cognition behaviors in human and animals. In the electronic domains, many emerging networks based on memristors or restickable oxide neuromorphic transistors have been proposed to realize associative learning and forgetting [31]-[38]. However, a promising approach for emulating the associative learning and forgetting with a PNN has not yet been addressed, which shows promises in processing speed and energy-efficiently.

In this paper, we propose a PNN based on VCSELs and STDP to emulate the associative learning and forgetting, and extend the PNN to realize the pattern recall for the first time. Based on the temporal coding [39]-[40], the input/output signals are encoded into spikes with precise timing by VCSEL-based neurons subject to double polarized optical injection (DOI) [4]-[6], [10]-[11], [15]-[18]. Thanks to the STDP rule, the associative learning and forgetting processes are well emulated in the PNN. Moreover, we further realize the pattern recall based on the photonic associative learning. The rest of the paper is organized as follows. The architecture of the PNN and theoretical model of the photonic neurons based on VCSELs are introduced in Section II. In Section III, temporal spike encoding and optical STDP are briefly shown. Then, the associative learning and forgetting processes are investigated carefully. The effects of time interval between a pair of two pre-synaptic spikes on the speed of associative learning and

This article has been accepted for publication in a future issue of this journal, but has not been fully edited. Content may change prior to final publication. Citation information: DOI 10.1109/JLT.2020.2995083, Journal of Lightwave Technology

forgetting are examined in detail. Finally, pattern recall based on the photonic associative learning is explored. Conclusions are presented in Section VI.

II. Theory and Model

A. Architecture of associative learning and forgetting

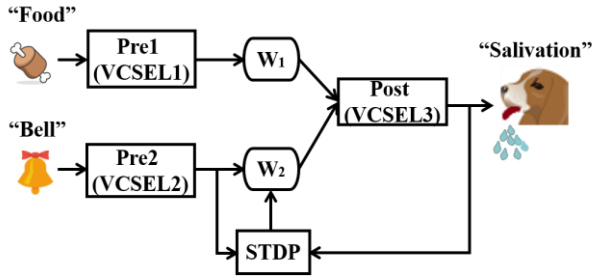

Fig. 1. Schematic diagram of associative learning and forgetting processes based on VCSELs and STDP. Pre1 and Pre2 encode food and bell stimulus respectively. Post represents salivation response. W_1 and W_2 represent the weight of photonic synapse. STDP is used to update synaptic weight.

The operation principles of Pavlovian associative learning and forgetting processes are introduced firstly [41]-[43]. Usually, feeding food and bell ringing are called unconditioned stimulus (US) and neutral stimulus (NS) respectively, while the salivation is called unconditioned response (UR). Initially, when only food is present, the dog can react with salivation. However, the dog cannot salivate when only bell rings. During the associative learning process, the dog is fed shortly after the bell rings repeatedly. After associative learning process, the dog salivates when only the bell rings, i.e., an association between bell and food is already established. Usually, the bell-elicited salivation is called conditioned response (CR) and bell ringing transfers from NS to conditioned stimulus (CS). Then, according to the conditioned inhibition or backward conditioning in biological system [38], [43], the dog is fed before the bell rings repeatedly during the forgetting process. The dog cannot salivate when only the bell rings after forgetting process, i.e., the established association between bell and food is forgotten.

The schematic diagram of the PNN to realize associative learning and forgetting processes is shown in Fig. 1. This PNN contains two VCSEL-based pre-synaptic neurons (Pre1 and Pre2) and one VCSEL-based post-synaptic neuron (Post). Here, the Pre1 (Pre2) encodes the feeding food (bell ringing). Post represents salivation response. For all VCSELs, the X-polarization (XP) is subject to continuous wave (CW) optical injection, which is introduced for eliminating the relax oscillation after the termination of stimulus pulse [6], [10]-[11], [16]-[17]. The stimulus pulses are injected into the Y-polarization (YP) of Pre1 and Pre2. The spikes generated by Pre1 and Pre2 are injected into the YP mode of Post. The weight of adaptive synapse between Pre1 (Pre2) and Post neurons, is denoted as W_1 (W_2), and can be modified according to STDP. Since spike (US) from Pre1 alone can make Post emit a spike (UR) during associative learning and forgetting processes, we can set W_1 to a large constant and $W_1 = 0.425$. Since spike (NS) from Pre2 alone cannot make the Post emit a spike before associative learning, the initial value of W_2 is quite small and $W_2 = 0.05$. During associative learning and forgetting processes, W_2 is modified according to spiking timing interval $\Delta t = t_{Post} - t_{Pre2}$, where t_{Pre2} (t_{Post}) denotes the spiking timing of Pre2 (Post). In this work, an ex-situ approach [25] is used for associative learning and forgetting, i.e., the STDP curve can be calculated in advance.

B. Model of photonic neurons: rate equations of VCSELs

In this work, the theoretical model of VCSEL-based photonic neuron is modified based on the well-known spin-flip model [44]. By incorporating the CW (pulsed) optical injection in the XP (YP) mode, the rate equations of three VCSELs are given by [4]-[6], [10]-11], [15]-[18]:

$$\frac{dE_{1x,2x}}{dt} = k(1+i\alpha)\left[\left(N_{1,2}-1\right)E_{1x,2x} + in_{1,2}E_{1y,2y}\right] - \left(\gamma_a + i\gamma_p\right)E_{1x,2x} + k_{xCW1,xCW2}E_{xCW1,xCW2}(t)e^{i\Delta\omega_x t} \quad (1)$$

$$\frac{dE_{1y,2y}}{dt} = k(1+i\alpha)\left[\left(N_{1,2}-1\right)E_{1y,2y} - in_{1,2}E_{1x,2x}\right] + \left(\gamma_a + i\gamma_p\right)E_{1y,2y} + k_{yPL1,yPL2}E_{yPL1,yPL2}(t)e^{i\Delta\omega_y t} \quad (2)$$

$$\frac{dE_{3x}}{dt} = k(1+i\alpha)\left[\left(N_3-1\right)E_{3x} + in_3E_{3y}\right] - \left(\gamma_a + i\gamma_p\right)E_{3x} + k_{xCW3}E_{xCW3}(t)e^{i\Delta\omega_x t} \quad (3)$$

$$\frac{dE_{3y}}{dt} = k(1+i\alpha)\left[\left(N_3-1\right)E_{3y} - in_3E_{3x}\right] + \left(\gamma_a + i\gamma_p\right)E_{3y} + k_{13y}E_{1y}(t-\tau_{13})e^{-i\omega_y\tau_{13}}e^{i\Delta\omega_{13}t} + k_{23y}E_{2y}(t-\tau_{23})e^{-i\omega_y\tau_{23}}e^{i\Delta\omega_{23}t} \quad (4)$$

$$\frac{dN_{1,2,3}}{dt} = -\gamma_e\left[N_{1,2,3}\left(1+\left|E_{1x,2x,3x}\right|^2+\left|E_{1y,2y,3y}\right|^2\right)-\mu_{1,2,3}\right] - \gamma_e\left[in_{1,2,3}\left(E_{1y,2y,3y}E^*_{1x,2x,3x} - E_{1x,2x,3x}E^*_{1y,2y,3y}\right)\right] \quad (5)$$

$$\frac{dn_{1,2,3}}{dt} = -\gamma_s n_{1,2,3} - \gamma_e\left[n_{1,2,3}\left(\left|E_{1x,2x,3x}\right|^2+\left|E_{1y,2y,3y}\right|^2\right)\right] - \gamma_e\left[iN_{1,2,3}\left(E_{1y,2y,3y}E^*_{1x,2x,3x} - E_{1x,2x,3x}E^*_{1y,2y,3y}\right)\right] \quad (6)$$

Where the subscripts 1, 2, and 3 represent Pre1, Pre2 and Post, respectively. $E_{x,y}$ are the slowly varying field of XP and YP. N represents the total carrier inversion between conduction and valence bands. n is difference between carrier inversions with opposite spins. The external CW (pulse) optical injection is characterized by $E_{xCW}(t)$ ($E_{yPL}(t)$) and $\Delta\omega_x$ ($\Delta\omega_y$) with injection strength k_{xCW} (k_{yPL}). The third (fourth) term in Eq. (4) means the injection from the YP mode of Pre1 (Pre2) into the YP mode of Post with coupling strength k_{13y} (k_{23y}), delay τ_{13} (τ_{23}) and center angular frequency detuning $\Delta\omega_{13}$ ($\Delta\omega_{23}$). k_{13y} (k_{23y}) represents the synaptic weight W_1 (W_2), and k_{13y}=k_rW_1 (k_{23y}=k_rW_2). Here, k_r is used to ensure the emission of the YP mode of Post. Note that, $\Delta\omega_x$ ($\Delta\omega_y$) is the difference of

angular frequency and $\Delta\omega_x = \omega_{xCW} - \omega_0$ ($\Delta\omega_y = \omega_{yPL} - \omega_0$), where $\omega_0 = (\omega_x + \omega_y)/2$ is the center frequency of two polarization outputs with $\omega_x = \omega_0 + \alpha\gamma_a - \gamma_p$, $\omega_y = \omega_0 + \gamma_p - \alpha\gamma_a$. $\Delta f_x = f_{xCW} - f_0$ ($\Delta f_y = f_{yPL} - f_0$) is the frequency detuning between the injected filed and the XP (YP) mode of VCSELs. Thus, $\Delta\omega_x = 2\pi\Delta f_x + \alpha\gamma_a - \gamma_p$ ($\Delta\omega_y = 2\pi\Delta f_y + \gamma_p - \alpha\gamma_a$). Besides, $\Delta\omega_{13}=2\pi\Delta f_{13}$ ($\Delta\omega_{23}=2\pi\Delta f_{23}$), where Δf_{13} (Δf_{23}) is the central frequency detuning between Pre1 (Pre2) and Post. Here, the noise is ignored for the sake of simplicity. Some typical parameters for 1550nm VCSEL [11] are defined in Table 1.

TABLE I
SOME TYPICAL PARAMETERS FOR VCSEL

Symbol	Quantity	Value
λ	lasing wavelength for all VCSELs	1550nm
k	field decay rate	125ns^{-1}
γ_a	linear dichroism	2ns^{-1}
γ_p	linear birefringence	192ns^{-1}
γ_e	the decay rate of N	1ns^{-1}
γ_s	spin-flip rate	1000ns^{-1}
α	linewidth enhancement factor	2.2
μ	normalized pump current	$\mu_1 = \mu_2 = 2.5$
$E_{xCW1,2,3}$	external CW optical injection	1
$k_{xCW1,2,3}$	injection strength of CW optical injection	70ns^{-1}
$k_{yPL1,2}$	injection strength of pulse optical injection	145ns^{-1}
$\tau_{13,23}$	coupling delay	1ns
k_r	part of coupling strength	100ns^{-1}
$\Delta f_{x1,2,3}$ ($\Delta f_{y1,2}$)	frequency detuning between the injected filed and the XP (YP) mode of VCSELs	1.1GHz (0GHz)

III. NUMERICAL RESULTS

A. Temporal spike encoding based on VCSEL

We numerically solve the rate equations by fourth-order Runge-Kutta method with an integration step of 1 ps. Figure 2 illustrates the temporal spike encoding result based on VCSEL under DOI [11]. Initially, the lasing (subsidiary) mode of free-running VCSEL is YP (XP). Then, $E_{xCW}(t)$ with $\Delta f_x = 1.1$GHz is injected into the XP mode of the VCSEL. Obviously, the lasing (subsidiary) mode of VCSEL changes from YP (XP) mode to XP (YP) mode, which is named polarization switching (PS). Then, $E_{yPL}(t)$ with $\Delta f_y = 0$GHz is injected into the YP mode of VCSEL. The lasing (subsidiary) mode of VCSEL changes from XP (YP) mode to YP (XP) mode again, which is named reverse polarization switching (reverse PS). As shown in Fig. 2, $E_{yPL}(t)$ can be encoded into neuron-like dynamics without unwanted relaxation oscillation based on the PS, which precisely computes the arrival of external stimulus [18]. Thus, we assume that the VCSEL emits a spike when $I_y \geq I_{yLth}$ with $I_{yLth} = 10$, and the VCSEL emits no spike when $I_y \leq I_{yFth}$ with $I_{yFth} = 0.03$. $t_{cPL} = 7$ns and $DT = 0.07$ns indicate center time and duration of $E_{yPL}(t)$, respectively. Here, the intensities are defined as $I_{x,y} = |E_{x,y}|^2$. Note, $E_{xCW}(t)$ is defined as a bias of a photonic neuron, and $E_{yPL}(t)$ is considered as US or NS in this paper. That is to say, the neuron-like dynamics is achieved based on the mechanisms of normal and reverse PS, which is different from the excitable VCSEL with saturable absorber (VCSEL-SA) that based on the excitability property [19], [27], [45].

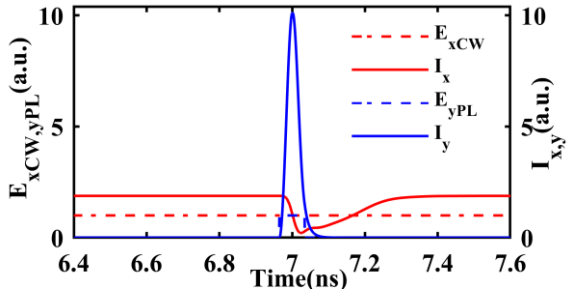

Fig. 2. Temporal spike encoding based on VCSELs under DOI. $E_{xCW} = 1$ with $\Delta f_x = 1.1$GHz ; $E_{yPL} = 1$ with $\Delta f_y = 0$. $t_{cPL} = 7$ns and $DT = 0.07$ns indicate center time and duration of E_{yPL}(t) , respectively. $\mu = 2.5$.

B. Photonic STDP based on VCSOA

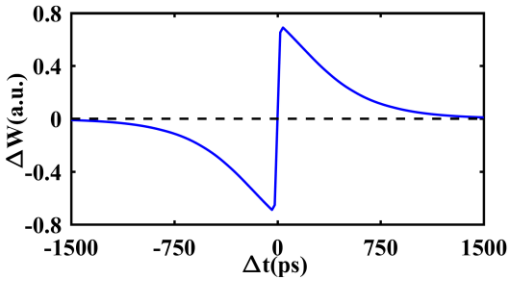

Fig. 3. The photonic STDP curve based on VCSOA. $\Delta\lambda_i = 0$nm and $\Delta\lambda_o = -0.05$nm . The black dashed line corresponds to $\Delta W = 0$.

Here, the details of photonic STDP based on a VCSOA had been presented in our previous work [26]. The calculated STDP curve is shown in Fig. 3 and shows that the amount of weight change $\Delta W > 0$ ($\Delta W < 0$) when $\Delta t > 0$ ($\Delta t < 0$). Usually, the section of STDP curve when $\Delta t > 0$ ($\Delta t < 0$) is called Long-term Potentiation (Depression) window, also known as LTP (LTD). In the PNN, the synaptic weight can be updated based on the stored $\Delta W(\Delta t)$ via an ex-situ learning approach. During the learning phase, the modification of synaptic weight from learning cycle X to $X+1$ is computed as follows [46]:

$$W(X+1) = W(X) + W_f \times \Delta W(\Delta t) \quad (7)$$

Where $W(X)$ and $W(X+1)$ are the weights of synapse at X-th and $(X+1)$-th learning cycles, respectively. W_f is learning rate, and $W_f = 0.05$ in this paper.

C. Associative learning and forgetting processes

In this section, the emulation of associative learning and forgetting processes based on the PNN are presented in Fig. 4.

This article has been accepted for publication in a future issue of this journal, but has not been fully edited. Content may change prior to final publication. Citation information: DOI 10.1109/JLT.2020.2995083, Journal of Lightwave Technology

Note, t_{Pre1L} (t_{Pre1F}) is the spiking time of Pre1 during the associative learning (forgetting) process.

Here, the whole process of associative learning and forgetting learning contains seven stages, and is presented in Fig. 4. Stage one (S1) and two (S2) represent the initial states. Stage three (S3) illustrates the associative learning process, and stage four (S4) shows associative test process. Stage five (S5) shows the forgetting process, and stage six (S6) represents forgetting test process. Stage seven (S7) is used to test whether the dog still remembers food after associative learning and forgetting processes. Note that, for the purpose of direct comparison, the x-axes for the Figs. 4(a2, b2, c2, d2, e2) is shifted to left by 1ns to compensate the transmission delay τ_{13} and τ_{23}. Besides, the corresponding weight update processes of W_2 for seven stages are also presented in Fig.5. For clarity, some typical parameters corresponding to Figs.4 and 5 are defined in Table 2.

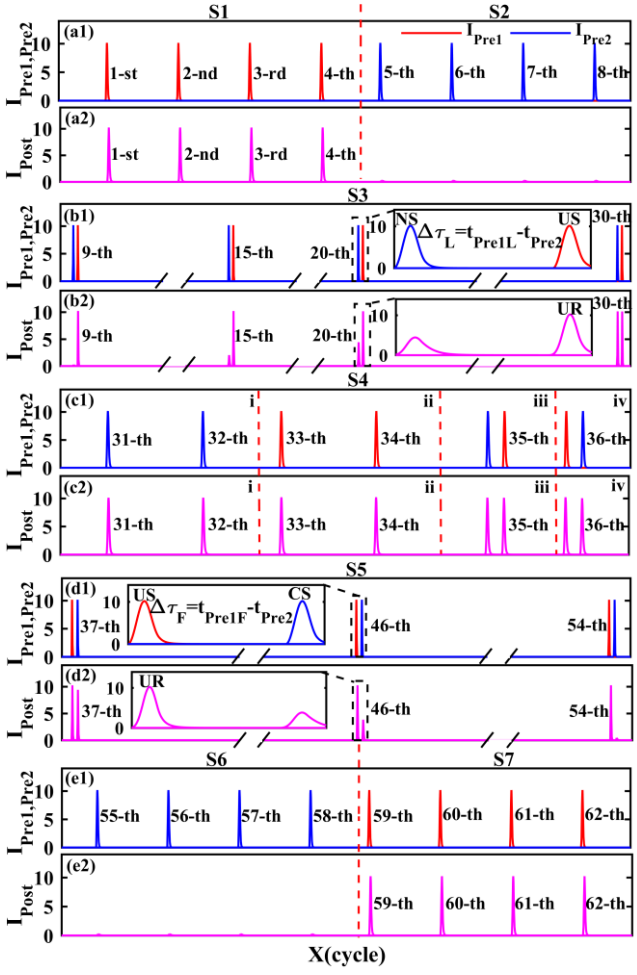

Fig. 4. Simulations of associative learning and forgetting processes. $E_{yPL1}=1$ for S1, S3, S4(ii,iii,iv), S5, S7; $E_{yPL1}=0$ for S2, S4(i), S6; $E_{yPL2}=1$ for S2, S3, S4(i,iii,iv), S5, S6; $E_{yPL2}=0$ for S1, S4(ii), S7; $\Delta\tau_L=0.35$ns for S3, S4(iii); $\Delta\tau_F=-0.35$ns for S4(iv), S5. In all cases, $\Delta f_{13}=0$GHz, $\Delta f_{23}=0$GHz, $\mu_3=2.5$.

As presented in Figs. 4(a1) and (a2), during S1 (S2), since W_1 (W_2) is (isn't) large enough, US (NS) from Pre1 (Pre2) alone can make the Post emit a (no) spike for each run. Besides, W_2 keeps constant in S1 (S2). In S3 which is shown in Figs. 4(b1) and (b2), Pre1 emits a spike (US) shortly after the Pre2 emits a spike (NS) repeatedly with $\Delta\tau_L$, which is presented in the inset of Fig. 4(b1). Since $t_{Post}\approx t_{Pre1L}$ before NS can trigger Post with a spike, $\Delta t=\Delta\tau_L=0.35$ns in S3. According to LTP window shown in Fig. 3, weight change $\Delta W(\Delta t)$ is positive when $\Delta t=0.35$ns. Note, the weight update amount for each run is set to a fixed value. Therefore, W_2 increases linearly as the learning cycle increases during the associative learning process. After X_L learning cycles, when the NS alone can make the Post emit a spike (CR), i.e., $I_{Post}\geq I_{yLth}$, the associative learning process stops. Obviously, a smaller X_L denotes a faster associative learning process. For simplicity, the intermediate process of S3 is not shown.

TABLE II
SOME TYPICAL PARAMETERS CORRESPONDING TO FIGS.4 AND 5

Symbol	Quantity	Value
$\Delta\tau_L$	$t_{Pre1L}-t_{Pre2}$	0.35ns
$\Delta\tau_F$	$t_{Pre1F}-t_{Pre2}$	-0.35ns
X_L	learning cycle X at which the NS can trigger the Post with a spike	22
X_F	learning cycle X at which the CS cannot trigger the Post with a spike	19
W_{2max}	W_2 at which the NS can trigger the Post with a spike	0.425

Note: in this work, $|\Delta\tau_L|=|\Delta\tau_F|$.

As presented in Figs. 4(c1) and (c2), S4 is the associative test process and consists of four sub-stages: (i) ((ii)) represents that NS (US) alone can make Post emit a spike named CR (UR). Besides, NS becomes CS and (ii) means that the dog still remembers the food after associative learning; (iii) and (iv) represent that Post can generate UR and CR independently with $\Delta\tau_L$ and $\Delta\tau_F$, respectively. The corresponding W_2 in S4 remains constant. We consider that the association between NS and US is established when the four sub-stages of S4 are all satisfied. Note that, the section (iv) is also the first cycle for the forgetting process.

S5 is shown in Figs. 4(d1) and (d2). Here, Pre1 emits a spike (US) before Pre2 emits a spike (CS) repeatedly with $\Delta\tau_F$, which is presented in the inset of Fig. 4(d1). Since US can trigger Post with a spike during the forgetting process, $t_{Post}\approx t_{Pre1F}$ and $\Delta t=\Delta\tau_F=-0.35$ns in S5. According to LTD window shown in Fig. 3, weight change $\Delta W(\Delta t)$ is negative when $\Delta t=-0.35$ns in S5. Similar to the associative learning process, the weight update amount for each run is the same. Thus, W_2 decreases linearly as the learning cycle increases during the forgetting process. When CS can't make the Post emit a spike after X_F learning cycles, i.e., I_{Post} triggered by the CS is less than the defined threshold I_{yFth}, forgetting process stops and the association is completely forgotten. The intermediate process of S5 is not shown for

This article has been accepted for publication in a future issue of this journal, but has not been fully edited. Content may change prior to final publication. Citation information: DOI 10.1109/JLT.2020.2995083, Journal of Lightwave Technology

simplicity. S6 and S7 are presented in Figs. 4(e1) and (e2). CS (US) from Pre2 (Pre1) alone can make the Post emit no (a) spike in S6 (S7), which means that the dog forgets (remembers) the bell (food) after the forgetting process. Then, CS becomes NS again in S6. Besides, W_2 in S6 and S7 also keeps constant.

That is to say, we have successfully emulated the associative learning and forgetting processes with the PNN consisting of the VCSELs based on the spin-flip model. But note that, the photonic neuron based on the mechanism of normal and reverse PS of VCSEL is not the same as the photonic neuron based on the excitability of VCSEL-SA [19], [27], [45]. For an excitable VCSEL-SA which is analogous to a leaky integrate-and-fire laser neuron, we have also performed similar calculation based on the same network architecture. Interestingly, we find that the PNN consisting of VCSEL-SA can also realize associative learning and forgetting with the help of STDP (not shown here).

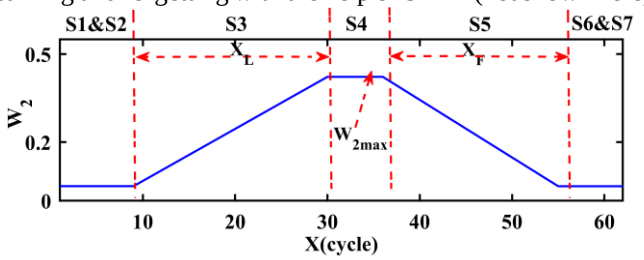

Fig. 5. The update process of W_2 in Fig.4. The learning cycle X (W_2) at which the NS can trigger the Post with CR is defined as X_L ($W_{2\max}$), X_F is value of learning cycles which the CS cannot trigger the Post with CR.

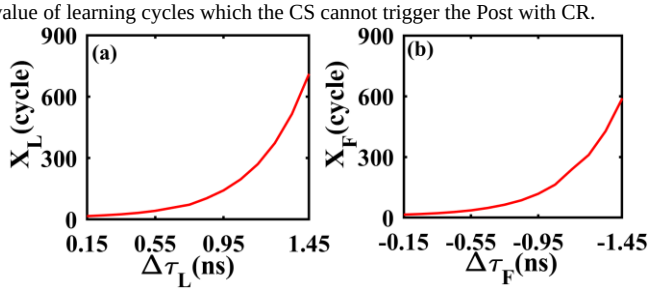

Fig. 6. Learning cycle X_L varies with $\Delta\tau_L$ (a) and learning cycle X_F varies with $\Delta\tau_F$ (b) when μ_3=3.5, $\Delta f_{13}=-4$GHz, $\Delta f_{23}=-8$GHz. In all cases, $E_{yPL1}=1$, $E_{yPL2}=1$. Other parameters are the same as S3 and S5 in Fig.4.

It has been demonstrated that a smaller time interval between NS and US leads to stronger association effect [47]-[48], i.e., the association becomes weaker as the time interval between NS and US increases. Next, we explore the effect of $\Delta\tau_L$ on the speed of associative learning and forgetting processes. As shown in Fig. 6(a) (Fig. 6(b)), X_L (X_F) increases as $\Delta\tau_L$ ($\Delta\tau_F$) increases (decreases). Namely, the speed of associative learning (forgetting) decreases as the $|\Delta\tau_L|$ increases. This phenomenon is because that, $|\Delta W|$ decreases as the $|\Delta\tau_L|$ increases according to the STDP curve in Fig. 3, while $W_{2\max}$, I_{yLth}, I_{yFth} remain constant with increasing $|\Delta\tau_L|$. In short, the time interval $\Delta\tau_L$ between two pre-spikes is the critical factor determining the speed of associative learning and forgetting. We also evaluate quantitatively the effects of bias current and central frequency detuning on the speed of associative learning and forgetting. It is found that, the learning speed is hardly affected by the bias current and central frequency detuning (not shown here).

Compared to the implementations of associative learning in the electronic counterparts [31]-[38], [49], photonic associative learning exhibits several advantages. Firstly, as shown in Fig. 6, X_L is 16 when $\Delta\tau_L=0.15$ns. The learning time for each run is about 0.22 ns by adding the time durations of US/NS ($\Delta\tau_L+DT$). Therefore, when $\Delta\tau_L=0.15$ns, the whole time of associative learning process is about 3.52 ns ($X_L\times 0.22$ns). In the electronic counterparts, the whole time of associative learning process is at least 16 μs [32]. Obviously, the speed of photonic associative learning is much faster than that of the electronic counterparts [31]-[38]. Secondly, there is lower crosstalk during photonic associative learning than that in the electronic domains [3]-[19], [49].

D. Pattern Recall based on associative learning

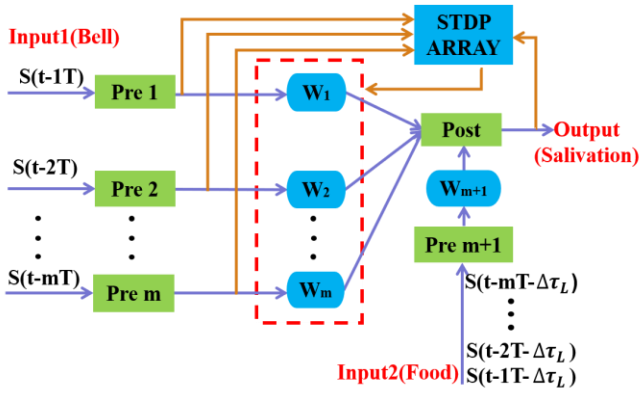

Fig.7. Schematic diagram of pattern recall. Pre 1-m and Pre $m+1$ are used to encode incomplete pattern and complete pattern respectively. Post encodes output of this network; W_m is the weight of photonic synapse. STDP ARRAY is used to update W_m. E_{yPLm} is determined by the m-th pixel of the patterns. Other parameters are the same as S3 in Fig.4.

TABLE III
SOME TYPICAL PARAMETERS CORRESPONDING TO FIG.7

Symbol	Quantity	Value
$\Delta\tau_{Lm}$	$t_{Pre2m}-t_{Pre1m}$	0.35ns
Δt_m	$t_{Postm}-t_{Pre1m}$	0.35ns
T	the encoding window	2ns
W_m	the initial value synaptic weight between the m-th Pre and Post	0.05
W_{m+1}	the constant value synaptic weight between Pre $m+1$ and Post	0.425

Subsequently, we further realize pattern recall based on associative learning [50]-[54]. The schematic diagram of pattern recall is presented in Fig. 7. Besides, some typical parameters corresponding to Fig.7 are defined in Table 3. The incomplete pattern is encoded by m Pres at the Input1 port. More precisely, when the value of the m-th pixel of incomplete pattern is 1 (0), the m-th Pre emit a (no) spike at the m-th encoding window and the corresponding spiking time is defined as t_{Pre1m}. On the other hand, the complete pattern is encoded by Pre m+1 at the Input2 port. When the

This article has been accepted for publication in a future issue of this journal, but has not been fully edited. Content may change prior to final publication. Citation information: DOI 10.1109/JLT.2020.2995083, Journal of Lightwave Technology

value of the m-th pixel of complete pattern is 1 (0), Pre m+1 emit a (no) spike at the m-th encoding window with $\Delta\tau_{Lm}$ later and the corresponding spiking time is defined as t_{Pre2m}. The result of pattern recall is represented by the response of Post, i.e., Post emit a (no) spike represents the value of pixel is 1 (0). According to associative learning, the spiking time t_{Postm} of Post at the m-th encoding window is equals to t_{Pre2m}. Thus, $\Delta t_m = \Delta\tau_{Lm}$. During the process of associative leaning, W_m at the m-th encoding window is updated according to the STDP curve in Fig. 3 and Δt_m. When W_m is larger than or equal to W_{m+1} after associative learning, Post can emit a spike at the m-th encoding window, i.e., the m-th pixel of incomplete pattern can be recovered. While W_m is smaller than W_{m+1}, the m-th pixel of incomplete pattern can't be recovered. Here, the patterns are binary images of size 20×20 pixels, which contain 400 pixels. Note, pixel value 1 and pixel value 0 represent white and black, respectively.

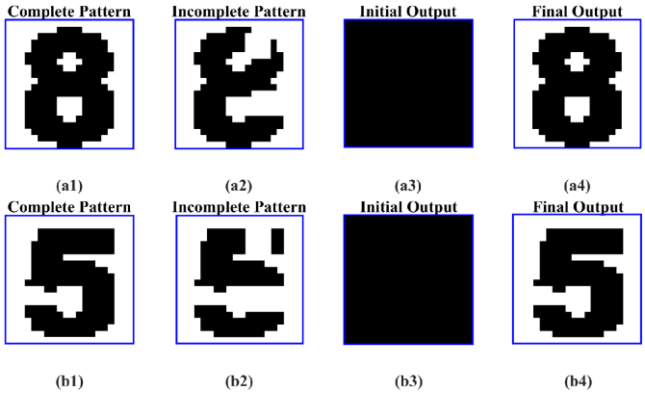

Fig. 8. (a1) and (b1) show complete pattern of number 8 and 5 respectively. (a2) and (b2) show incomplete pattern of number 8 and 5 respectively. (a3) and (b3) show initial output before learning. (a4) and (b4) show final output after learning. The blue box is just for visualization and has no practical meaning.

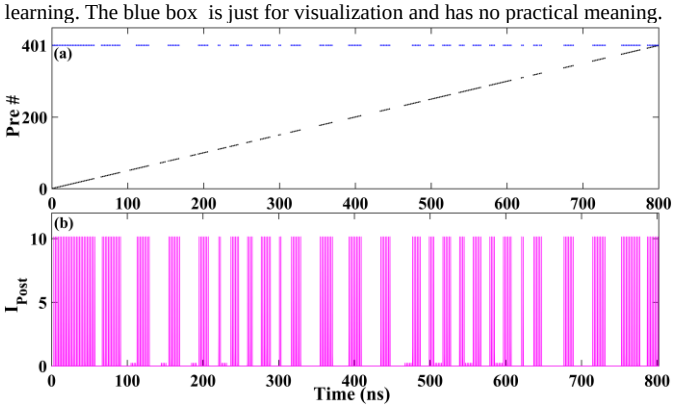

Fig. 9. (a) Spatiotemporal spike encoding of number 8 at the input ports. Pre 1-400 encode the incomplete pattern; Pre 401 encodes the complete pattern (b) The response of the Post corresponding to number 8 at the output port. There is a (no) spike when $I_y \geq I_{yth}$ ($I_y \leq I_{yFth}$) in the encoding window.

For instance, as shown in Fig. 9(a), Pre 1-400 encode the incomplete pattern of number 8 in Fig. 8(a2) and Pre 401 encodes the complete pattern of number 8 in Fig. 8(a1). Besides, we transfer the dimensions of the output from 1×400 to 20×20 for visualization. Figure 8(a3) shows the initial output when incomplete pattern of number 8 is entered into Pre 1-400 alone before associative learning process. Obviously, the incomplete pattern cannot be recovered. Correspondingly, the final output after associative learning process is shown in Fig. 9(b), and the visualization result is shown in Fig. 8(a4). It is clear that, the final output is almost the same as the complete pattern in Fig. 8(a1), i.e., the incomplete pattern can be recovered after associative learning and pattern recall is realized. The evolution of W_m corresponding to the pattern recall of number 8 is presented in Fig. 10(a). The initial value and final value of W_m corresponding to the pattern recall of number 8 are shown in Fig. 10(c). It shows that the value of W_m is so high (low) that pattern recall can (can't) be realized after (before) 22 cycles of learning, which verifies the feasibility of this network for pattern recall. Without loss of generality, we also consider another representative cases of pattern recall. The pattern recall process of number 5 and the corresponding weight evolution are shown in Figs. 8(b1, b2, b3, b4) and Figs. 10(b) and (d). It is verified that, pattern recall can be achieved with the proposed photonic associative learning network.

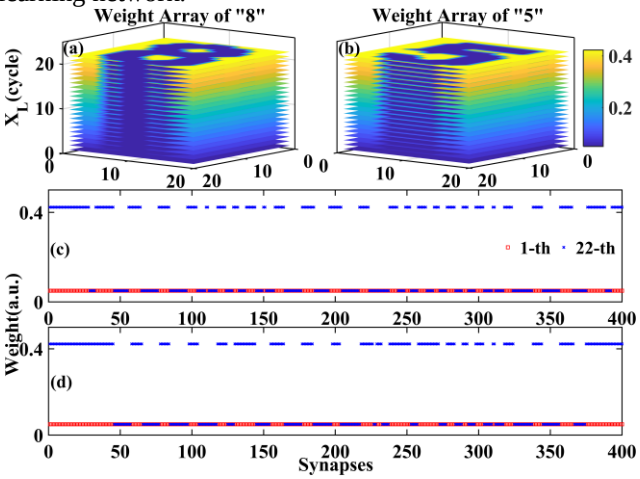

Fig. 10. (a) The change process of synaptic weight W_m for number 8, (b) the change process of synaptic weight W_m for number 5, (c) the initial value and final value of W_m corresponding to the pattern recall of number 8, (d) the initial value and final value of W_m corresponding to the pattern recall of number 5.

IV. Conclusion

In this work, we numerically realized associative learning and forgetting using the PNN based on VCSELs and STDP. Then, we demonstrated that the time interval between two pre-spikes is the critical factor determining the speed of associative learning and forgetting. Finally, based on associative learning, we demonstrated the feasibility of the PNN for pattern recall, which indicates potential applications for the PNN in flexible neuromorphic cognitive platforms. Besides, the high speed of the PNN is beneficial to some real-time processing system. Moreover, the ability of PNN to correlate different memories to the same fact or event, promises the feasibility of modeling intelligent functions of human brains and shows good prospects for brain-inspired and

large-scale integrated computing.

REFERENCES

[1] A. S. Cassidy, J. Georgious, A. G. Andreou, "Design of silicon brains in the nano-CMOS era: spiking neurons, learning synapses and neural architecture optimization," *Neural Netw.*, vol. 45, pp. 4-26, Sept. 2013.

[2] M. Don, "Neuromorphic computing gets ready for the (really) big time," *Commun. ACM.*, vol. 57, no. 6, pp. 13-15, Jun. 2014.

[3] M. A. Nahmias, B. J. Shastri, A. N. Tait, T. F. de Lima, P. R. Prucnal, "Neuromorphic photonics," *Opt. Photonics News.*, vol. 29, no. 1, pp. 34-41, Jan. 2018.

[4] A. Hurtado, I. D. Henning, and M. J. Adams, "Optical neuron using polarization switching in a 1550 nm-VCSEL," *Opt. Exp.*, vol. 18, no. 24, pp. 25170–25176, Nov. 2010.

[5] A. Hurtado, K. Schires, I. D. Henning, and M. J. Adams, "Investigation of vertical cavity surface emitting laser dynamics for neuromorphic photonic systems," *Appl. Phys. Lett.*, vol. 100, no. 10, Mar. 2012, Art no. 103703.

[6] M. Sciamanna and K. Panajotov, "Two-mode injection locking in vertical-cavity surface-emitting lasers," *Opt. Lett.*, vol. 30, no. 21, pp. 2903–2905, Nov. 2005.

[7] A. Hurtado, J. Javaloyes, "Controllable spiking patterns in long-wavelength vertical cavity surface emitting lasers for neuromorphic photonics systems," *Appl. Phys. Lett.*, vol. 107, no. 24, Dec. 2015, Art no. 241103.

[8] W. L. Zhang, W. Pan, B. Luo, X. H. Zou, and M. Y. Wang, "Polarization switching and hysteresis of VCSELs with time-varying optical injection," *IEEE J. Sel. Topics Quantum Electron.*, vol. 14, no. 3, pp. 889–894, May/Jun. 2008.

[9] S. Y. Xiang, W. Pan, B. Luo, L. Yan, X. Zou, and N. Li, "Influence of variable-polarization optical feedback on polarization switching properties of mutually-coupled VCSEL," *IEEE J. Sel. Topics Quantum Electron.*, vol. 19, no. 4, Jul./Aug. 2013, Art no. 1700108.

[10] P. Pérez, A. Valle, L. Pesquera, and A. Quirce, "All-optical inverter based on polarization switching in VCSELs subject to single and dual optical injection," *IEEE J. Sel. Topics Quantum Electron.*, vol. 19, no. 4, Jul./Aug. 2013, Art no. 1700408.

[11] M. F. Salvide, M. S. Torre, I. D. Henning, M. J. Adams, A. Hurtado, "Dynamics of normal and reverse polarization switching in 1550-nm VCSELs under single and double optical injection," *IEEE J. Sel. Top. Quantum Electron.*, vol. 21, no. 6, Nov./Dec. 2015.

[12] N. Q. Li, H. Susanto, B. Cemlyn, I. D. Henning, M. J. Adams, "Secure communication systems based on chaos in optically pumped spin-VCSELs," *Opt. Lett.*, vol. 42, no 17, pp. 3494-3497, Sept. 2017.

[13] N. Jiang, C. P. Xue, D. Liu, Y. X. Lv, K. Qiu, "Secure key distribution based on chaos synchronization of VCSELs subject to symmetric random-polarization optical injection," *Opt. Lett.*, vol. 42, no. 6, pp. 1055-1058, Mar. 2017.

[14] A. Quirce *et al*., "Polarization switching and injection locking in vertical cavity surface-emitting lasers subject to parallel optical injection," *Opt. Lett.*, vol. 41, no. 11, pp. 2664–2667, Jun. 2016.

[15] S. Y. Xiang, A. J. Wen, W. Pan, "Emulation of spiking response and spiking frequency property in VCSEL-based photonic neuron," *IEEE Photonics J.*, vol. 8, no. 5, Oct. 2016. Art. No. 1504109.

[16] T. Deng, J. Robertson, and A. Hurtado, "Controlled propagation of spiking dynamics in vertical-cavity surface-emitting lasers: towards neuromorphic photonic networks," *IEEE J. Sel. Topics Quantum Electron.*, vol. 23, no. 6, Nov./Dec. 2017, Art no. 1800408.

[17] S. Y. Xiang *et al*, "Cascadable neuron-like spiking dynamics in coupled VCSELs subject to orthogonally polarized optical pulse injection," *IEEE J. Sel. Top. Quantum Electron.*, vol. 23, no. 6, Nov/Dec. 2017. Art. No. 1700207.

[18] S. Y. Xiang, Y. H. Zhang, X. X. Guo, A. J. Wen, Y. Hao, "Photonic generation of neuron-like dynamics using VCSELs subject to double polarized optical injection," *J. Lightwave Technol.*, vol. 36, no. 19, pp. 4227-4234, Oct. 2018.

[19] Y. H. Zhang, S. Y. Xiang, J. K. Gong, X. X. Guo, A. J. Wen, and Y. Hao, "Spike encoding and storage properties in mutually coupled vertical-cavity surface-emitting lasers subject to optical pulse injection," *Appl. Opt.*, vol. 57, no. 7, pp. 1731-1737, Mar. 2018.

[20] S. Xiang, Z. Ren, Y. Zhang, Z. Song, and Y. Hao, "All-optical neuromorphic XOR operation with inhibitory dynamics of a single photonic spiking neuron based on VCSEL-SA," *Opt. Lett.*, vol. 45, no. 5, pp. 1104-1107, Feb. 2020.

[21] P. J. Sjostrom, E. A. Rancz, A. Roth, M. Hausser, "Dendritic excitability and synaptic plasticity," *Physiol Rev.*, vol. 88, no. 2, pp. 769-840, Apr. 2008.

[22] Q. S. Ren, K. M. Kolwankar, A. Samal, and J. Jost, "STDP-driven networks and the C. elegans neuronal network," *Physica A.*, vol. 389, no. 18, pp. 3900–3914, Sep. 2010.

[23] M. P. Fok, Y. Tian, D. Rosenbluth, P. R. Prucnal, "Pulse lead/lag timing detection for adaptive feedback and control based on optical spike-timing-dependent plasticity," *Opt. Lett.*, vol. 38, no. 4, pp. 419-421, Feb. 2013.

[24] Q. S. Ren, Y. L. Zhang, R. Wang, J. Y. Zhao, "Optical spike-timing-dependent plasticity with weight-dependent learning window and reward modulation," *Opt. Exp.*, vol. 23, no. 19, pp. 25247-25258, Sept. 2015.

[25] R. Toole, A. N. Tait, T. F. de Lima, A. N. Tait, B. J. Shastri, P. R. Prucnal, and M. P. Fok, "Photonic implementation of spike-timing-dependent plasticity and learning algorithms of biological neural systems," *J. Light. Technol.*, vol. 34, no. 2, pp. 470-476, Jan. 2016.

[26] S. Y. Xiang, J. K. Guo, Y. H. Zhang, X. X. Guo, Y. N. Han, A. J. Wen, and Y. Hao, "Numerical implementation of wavelength-dependent photonic spike timing dependent plasticity based on VCSOA." *IEEE J. Quantum Electron.*, vol. 54, no. 6, Dec. 2018, Art. no. 8100107.

[27] S. Y. Xiang, Y. H. Zhang, J. K. Guo, X. X. Guo, L. Lin, Y. Hao, "STDP-based unsupervised spike pattern in a photonic spiking neural network with VCSELs and VCSOAs." *IEEE J. Sel. Top. Quantum Electron.*, vol. 25, no. 6, Nov./Dec. 2019, Art. no. 1700109.

[28] V. A. Pammi, K. Alfaro-Bittner, M. G. Clerc, and S. Barbay, "Photonic computing with single and coupled spiking micropillar lasers," *IEEE J. Sel. Top. Quantum Electron.*, vol. 26, no. 1, p. 1500307, Jan./Feb. 2020.

[29] J. Robertson, E. Wade, Y. Kopp, J. Bueno, and A. Hurtado, "Toward neuromorphic photonic networks of ultrafast spiking laser neurons," *IEEE J. Sel. Top. Quantum Electron.*, vol. 26, no. 1, p. 7700715, Jan./Feb. 2020.

[30] H.-T. Peng, G. Angelatos, T. Ferreira de Lima, M. A. Nahmias, A. N. Tait, S. Abbaslou, B. J. Shastri, and P. R. Prucnal, "Temporal information processing with an integrated laser neuron," *IEEE J. Sel. Top. Quantum Electron.*, vol. 26, no. 1, p. 5100209, Jan./Feb. 2020.

[31] L. Chen, C. D. Li, X. Wang, S. K. Duan, "Associate learning and correcting in a memristive neural network," *Neural Comput. Appl*., vol. 22, no. 6, pp. 1071-1076, Feb. 2012.

[32] Y. Li, L. Xu, Y. P. Zhong, Y. X. Zhou. S. J. Zhong, Y. Z. Hu, L. O. Chua, X. S. Miao, "Associative learning with temporal contiguity in a memristive circuit for large-scale neuromorphic networks," *Adv. Electron. Mater.*, vol. 1, no. 8, Aug. 2015, Art. no. 1500125.

[33] X. Y. Liu, Z. G. Zeng, S. P. Wen, "Implementation of memristive neural network with full-function Pavlov associative memory," *IEEE Trans. Circuits Syst. I-Regul. Pap*., vol. 63, no. 9, pp. 1454-1463, Sept. 2016.

[34] L. D. Wang, H. F. Li, S. K. Duan, T. W. Huang, H. M. Wang, "Pavlov associative memory in a memristive neural network and its circuit implementation," *Neurocomputing.*, vol. 171, pp. 23-29, Jan. 2016.

[35] X. F. Hu, S. K. Duan, G. R. Chen, L. Chen, "Modeling affections with memristor-based associative memory neural networks," *Neurocomputing.*, vol. 223, pp. 129-137, Feb. 2017.

[36] L. Yang, Z. G. Zeng, S. P. Wen, "A full-function Pavlov associative memory implementation with memristance changing circuit," *Neurocomputing.*, vol. 272, pp. 513-519, Jan. 2018.

[37] X. Q. Lv *et al*. (2017. Oct). Guiyang, Guizhou, China. A neural network circuit with associative learning and forgetting process based on memristor neuromorphic device. Presented at ASICON. [Online]. Available: https://ieeexplore_ieee.xilesou.top/abstract/document/8252449

[38] F. Yu, L. Q. Zhu, H. Xiao, W.T. Gao, Y. B. Guo, "Restickable oxide neuromorphic transistors with spike-timing-dependent plasticity and Pavlovian associative learning activities," *Adv. Electron. Mater.*, vol. 28, no. 44, Oct. 2018, Art. no. 1804025.

[39] Z. F. Mainen, T. J. Sejnowski, "Reliability of spike timing in neocortical neurons," *Science.*, vol. 268, no. 5216, pp. 1503-1506, Jun. 1995.

[40] J. Gautrais, S. Thorpe, "Rate coding versus temporal order coding: a theoretical approach," *Biosystems.*, vol. 43, no. 1-3, pp. 57-65, Nov.1998.

[41] I. P. Pavlov, "Lectures on conditioned reflexes (Vol. II) ," *POSTGRAD MED J.*, vol. 18, no. 194, pp. 28, Jan, 1942.

[42] M. S. Fanselow, A. M. Poulos, "The neuroscience of mammalian associative learning," *Annu. Rev. Psychol.*, vol. 56, pp. 207-234, Feb. 2005.

[43] R. C. Chang, S. Stout, R. R. Miller, "Comparing excitatory backward and forward conditioning," *Q. J. Exp. Psychol.*, vol. 57, no. 1, pp. 1-23, Jan. 2004.

[44] J. Martin-Regalado, F. Prati, M. San Miguel, N.B. Abraham, "Polarization properties of vertical-cavity surface-emitting lasers," *IEEE J. Quantum Electron.*, vol. 33, no. 5, pp. 765-783, May. 1997.
[45] M. A. Nahmias, B. J. Shastri, A. N. Tait, and P. R. Prucnal, "A leaky integrate-and-fire laser neuron for ultrafast cognitive computing," *IEEE J. Sel. Top. Quantum Electron.* vol. 19, no. 5, Sep./Oct. 2013, Art. no. 1800212.
[46] R. Guyonneau, R. VanRullen, S. J. Thorpe, "Neurons tune to the earliest spikes through STDP," *Neural Comput.*, vol. 17, no. 4, pp. 859-879, Apr. 2005.
[47] K. Kirkpatrick, P. D. Balsam, "Associative learning and timing," *Curr. Opin. Behav. Sci.*, vol. 8, pp. 181-185, Apr. 2016.
[48] J.W. Sun, G. Y. Han, Z. G. Zeng, Y. F. Wang, "memristor-based neural network circuit of full-function Pavlov associative memory with time delay and variable learning rate," unpublished.
[49] X. Y. Wu *et al*, "A CMOS spiking neuron for brain-inspired neural networks with resistive synapses and in situ learning," *IEEE Trans. Circuits Syst.*, vol. 62, no. 11, pp. 1088-1092, Nov. 2015.
[50] D. Kuzum *et. al*, (Dec. 2011). Washington, DC, USA. Energy efficient programming of nanoelectronic synaptic devices for large-scale implementation of associative and temporal sequence learning. Presented at IEDM. [Online]. Available: https://ieeexplore_ieee.xilesou.top/abstract/document/6131643
[51] S. Kumar, M. P. Singh, "Pattern recall analysis of the Hopfield neural network with a genetic algorithm," *Comput. Math. Appl.*, vol. 60, no. 4, pp. 1049-1057, Aug. 2010.
[52] K. Fukushima, "Neural network model for selective attention in visual pattern recognition and associative recall," *Appl. Optics.*, vol. 26, no. 23, pp. 4985-92, Dec. 1987.
[53] B. Graham, D. Willshaw, "Improving recall from an associative memory," *Biol. Cybern.*, vol. 72, no. 4, pp. 337-346, Mar. 1995.
[54] N. Crook, W. J. Goh, M. Hawarat, "Pattern recall in networks of chaotic neurons," *Biosystems.*, vol. 87, no. 2-3, pp. 267-274, Feb. 2007.

Suhong Wang was born in Jiangsu, China, in1994. She is currently working toward the M.S. degree from Xidian University, Xi'an, China. Her research interests include the vertical cavity surface-emitting lasers and neuromorphic photonic systems.

Shuiying Xiang was born in Jiangxi, China, in 1986. She received the Ph.D. degree from Southwest Jiaotong University, Chengdu, China, in 2013. She is currently a Professor with the State Key Laboratory of Integrated Service Networks, Xidian University, Xi'an, China. She is the author or coauthor of more than 100 research papers. Her research interests include neuromorphic photonic systems, brain-inspired information processing, spiking neural network, vertical cavity surface-emitting lasers, and semiconductor lasers dynamics.

Genquan Han was born in Hengshui, China, in 1979. He received the B.Eng. degree from Tsinghua University, Beijing, China, and the Ph.D. degree from the Institute of Semiconductors, Chinese Academy of Sciences, Beijing, in 2008. He is currently a Professor with Xidian University, Xi'an, China. His current research interests include advanced CMOS, photonics devices, and wide bandgap materials and devices.

Ziwei Song was born in Henan, China, in1996. She is currently working toward the M.S. degree from Xidian University, Xi'an, China. Her research interests include the vertical cavity surface-emitting lasers and neuromorphic photonic systems.

Zhenxing Ren was born in Shannxi, China, in1996. He is currently working toward the M.S. degree from Xidian University, Xi'an, China. His research interests include the vertical cavity surface-emitting lasers and neuromorphic photonic systems.

Aijun Wen was born in Shannxi, China, in 1968. He received the Ph.D. degree from Xidian University, Xi'an, China, in 1998. He is a Professor with the State Key Laboratory of Integrated Service Networks, Xidian University, Xi'an, China. His current research interests include microwave photonics and optical communication.

Yue Hao was born in the city of Chongqing, China, in 1958. He received the Ph.D. degree from Xi'an Jiao tong University, Xi'an, China, in 1991.
He is currently a Professor at State Key Discipline Laboratory of Wide Bandgap Semiconductor Technology, the School of Microelectronics, Xidian University, Xi'an, China. His research interests include wide forbidden band semiconductor materials and devices.